THE JOURNAL OF BIOLOGICAL CHEMISTRY VOL. 284, NO. 33, pp. 22067–22078, August 14, 2009

mTOR/S6 Kinase Pathway Contributes to Astrocyte Survival during Ischemia*

Received for publication, March 23, 2009, and in revised form, June 15, 2009 Published, JBC Papers in Press, June 17, 2009, DOI 10.1074/jbc.M109.033100

María Dolores Pastor[‡], Isaac García-Yébenes[§], Noelia Fradejas[‡], José Manuel Pérez-Ortiz[‡], Silvia Mora-Lee[‡], Pedro Tranque[‡], María Ángeles Moro[§], Mario Pende[¶], and Soledad Calvo[‡1]

From the [‡]Department of Medical Sciences, Medical School, Universidad de Castilla La Mancha, 02006 Albacete, Spain, the [§]Department of Pharmacology, Medical School, Universidad Complutense de Madrid, 28040 Madrid, Spain, and [¶]INSERM U845, Université Paris Descartes, 75015 Paris, France

Neurons are highly dependent on astrocyte survival during brain damage. To identify genes involved in astrocyte function during ischemia, we performed mRNA differential display in astrocytes after oxygen and glucose deprivation (OGD). We detected a robust down-regulation of S6 kinase 1 (S6K1) mRNA that was accompanied by a sharp decrease in protein levels and activity. OGD-induced apoptosis was increased by the combined deletion of S6K1 and S6K2 genes, as well as by treatment with rapamycin that inhibits S6K1 activity by acting on the upstream regulator mTOR (mammalian target of rapamycin). Astrocytes lacking S6K1 and S6K2 (S6K1;S6K2$^{-/-}$) displayed a defect in BAD phosphorylation and in the expression of the anti-apoptotic factors Bcl-2 and Bcl-xL. Furthermore reactive oxygen species were increased while translation recovery was impaired in S6K-deficient astrocytes following OGD. Rescue of either S6K1 or S6K2 expression by adenoviral infection revealed that protective functions were specifically mediated by S6K1, because this isoform selectively promoted resistance to OGD and reduction of ROS levels. Finally, "*in vivo*" effects of S6K suppression were analyzed in the permanent middle cerebral artery occlusion model of ischemia, in which absence of S6K expression increased mortality and infarct volume. In summary, this article uncovers a protective role for astrocyte S6K1 against brain ischemia, indicating a functional pathway that senses nutrient and oxygen levels and may be beneficial for neuronal survival.

Astrocytes are the most abundant cells in the central nervous system. Their functions are crucial for central nervous system homeostasis, because they provide trophic, metabolic, and antioxidant support to neurons. In addition, astrocytes show the ability to modulate synaptic activity and are responsible for preserving neuronal integrity in conditions of disease and injury. In this regard, recent evidence indicates that they are protective for neurons during cerebral ischemia (1). As there is a growing consensus that astrocyte dysfunction may compromise the ability of neurons to survive, the need for studies that clarify the molecular mechanisms involved in the astrocytic response to ischemia is plainly justified.

Among the intracellular pathways that integrate signals from nutrients and oxygen, the mammalian target of rapamycin (mTOR)[2] kinase plays an evolutionary conserved role in the regulation of cell growth, proliferation, survival, and metabolism (2). mTOR exists in the cell in at least two distinct complexes with different partners, mTORC1 and mTORC2. The activity of mTORC1 is exquisitely sensitive to the energy status of the cell and is blocked by the macrolide antibiotic rapamycin. Glucose and oxygen deprivation inhibits mTORC1 activity, respectively, through the regulation of AMP-activated kinase and REDD1/REDD2 proteins (3–5). These factors favor the action of the tuberous sclerosis proteins TSC1 and TSC2, which suppress mTORC1 by forming a complex with GTPase-activating protein (GAP) activity for the small GTPase Rheb (6).

In turn, mTORC1 phosphorylates at least three distinct classes of substrates, the eIF4E-binding proteins (4EBP-1 to -3), the ribosomal protein S6 kinases (S6K1 and S6K2) and the serum- and glucocorticoid-inducible kinase 1. However, the pathophysiological role of the mTOR pathway during hypoxia-induced brain damage and the involvement of the distinct mTOR effectors remain to be established.

The anabolic actions of the mTOR pathway may in part depend on the regulation of protein synthesis. mTOR associates with the translation initiation factor eIF3 (7). In turn the mTORC1 substrates 4EBPs interact with the cap-binding protein eIF4E (8), while S6Ks phosphorylate the ribosomal protein rpS6 and eIF4B (9, 10). However loss of function mouse mutants of 4EBPs and S6Ks failed to uncover a role of these effectors in global protein synthesis during resting conditions, while instead suggesting an involvement in energy homeostasis and mitochondrial function (11–13). Therefore, mTOR plays critical anabolic and energetic functions still poorly understood, raising the appealing possibility that hypoxia-induced down-regulation of the mTOR pathway could be linked to brain damage. In this regard, S6K, besides stimulating phosphoryla-

* This work was supported by the Spanish Ministry of Education and Science (Grant BFU2006-14267) and Junta de Comunidades de Castilla-La Mancha (Grants PAI05-017 and PCI-08-0101-8639) (to S. C.).

[1] To whom correspondence should be addressed: Facultad de Medicina, Universidad de Castilla La Mancha, Avda. de Almansa 14, 02006 Albacete, Spain. Tel.: 34-967-599-200; Fax: 34-967-599-324; E-mail: soledad.calvo@uclm.es.

[2] The abbreviations used are: mTOR, mammalian target of rapamycin; GAP, GTPase-activating protein; S6K1, -2, S6 kinase 1 and 2; 4EBP, eIF4E-binding protein; OGD, oxygen and glucose deprivation; H2DCF-DA, dichlorodihydrofluorescein diacetate; DMEM, Dulbecco's modified Eagle's medium; MCAO, middle cerebral artery occlusion; RT, reverse transcription; GAPDH, glyceraldehyde-3-phosphate dehydrogenase; PBS, phosphate-buffered saline; TRITC, tetramethylrhodamine isothiocyanate; MTT, 3-(4,5-dimethylthiazol-2-yl)-2,5-diphenyltetrazolium bromide; PI, propidium iodide; m.o.i., multiplicity of infection.

tion of the ribosomal proteins rpS6 and eIF4B, has been shown to inactivate the anti-apoptotic factor BAD and the insulin receptor substrate IRS (13, 14), demonstrating additional targets that are not directly involved in protein synthesis and may be relevant for the physiological action of the pathway. Moreover, S6K activity is decreased in *in vivo* paradigms of global and focal brain ischemia (15–17); whereas insulin-activated cardioprotection during ischemia/reoxygenation-induced injury is linked to S6K activation (18).

Here we show that oxygen and glucose deprivation (OGD) decreases S6K1 mRNA levels in astrocyte cultures, leading to a reduction of S6K1 protein and activity. S6K loss of function leads to increased astrocyte death during ischemia, impairment of protein synthesis recovery, unbalance between mitochondrial pro- and anti-apoptotic factors and rise in ROS levels. Finally we reveal an effect of S6K suppression on mouse mortality and infarct volume following permanent middle cerebral artery occlusion. Our data indicate a novel role of S6K1 promoting astrocyte survival, protein synthesis, and brain protection in conditions of ischemic stress.

EXPERIMENTAL PROCEDURES

Chemicals

Dichlorodihydrofluorescein diacetate (H2DCF-DA) and Annexin V conjugated with Alexa Fluor 488 were purchased from Molecular Probes (Eugene, OR). Fetal bovine serum and glutamine were obtained from Invitrogen. Anti-S6K1, anti-phospho-Thr-389 S6K1, anti-phospo-Ser235/236 S6, anti-Bad, and anti-phospho-Ser-136 Bad Primary antibodies were provided by Cell Signaling. Monoclonal antibodies against S6K2 were previously described (9). Rapamycin was from Calbiochem. Anti-Bad antibody for immunoprecipitation, and all other chemicals were purchased from Sigma unless otherwise stated.

Animals and Primary Astrocyte Cultures

Generation of S6K1- and S6K2-deficient mice S6K1;2$^{-/-}$ has been previously described (9). Animals were initially in the mixed C57/Bl6-129Ola genetic background and then backcrossed ten times to a "pure" C57/Bl6 background. Primary cultures of astroglial cells were also prepared as mentioned before (19, 20) with minor modifications. Briefly, cortices from 1-day-old mouse pups were aseptically removed, minced, dissociated by trypsinization, and maintained in Dulbecco's modified Eagle's medium (DMEM) supplemented with 10% fetal bovine serum and penicillin/streptomycin. Fourteen days after plating, the flasks were shaken for 15–18 h at 37 °C to remove oligodendroglial and microglial cells. Astrocytes were then detached by trypsinization and plated either on culture dishes or poly-L-lysine-coated glass coverslips in supplemented DMEM. All experiments were performed 2–3 days after cells were re-plated.

Flow Cytometry for Cell Size Measurement

Astrocytes were dispersed by trypsinization, and the resulting single cell suspension was immediately used for cell size measurement. Relative cell size was assessed in 10,000-cell samples using a BD-LSR flow cytometer (BD Biosciences). Forward scatter height histograms were plotted, and mean values were calculated using CellQuest software, according to the manufacturer's instructions.

Ischemia Models

In Vitro OGD—Ischemia was induced following a formerly reported method (19) using an anaerobic chamber. Glucose- and serum-free DMEM was made anoxic by aeration with 99.95% N_2 for 30 min, and subsequently saturated with 5% CO_2 in N_2 for a further 20-min period. 24-h serum-starved astrocyte cultures were washed three times with ischemia media and maintained at 37 °C inside the ischemic chamber incubator. At the end of the designated period, medium was replaced and cells were returned to a normal culture incubator.

Permanent MCAO—Experiments were performed on 3-month-old male wild-type and S6K1;2$^{-/-}$ mice. They were anesthetized with 5% isoflurane (in 70%N_2O, 30%O_2) for induction and 1.5% isoflurane for maintenance, and the rectal temperature was kept at 37 °C with a heating pad. The middle cerebral artery was exposed and occluded permanently by electrocoagulation (21). All procedures conformed to the Committee of Animal Care at the Universidad Complutense of Madrid according with European Union rules (86/609/CEE, 2003/65/CE, and RD 1201/2005). Brains were removed 2 or 7 days after middle cerebral artery occlusion (MCAO), cut into seven 1-mm-thick coronal brain slices (Brain Matrix, WPI-Europe, Aston, Stevenage, UK), and stained in 0.2 M phosphate buffer containing 2% 2,3,5-triphenyltetrazolium chloride. Infarct size (mm^3) was determined as previously described (22) and expressed as infarct volume per 100 mg of tissue to compensate for the differences in brain size between S6K1;2$^{-/-}$ and wild-type mice.

RNA Isolation

Total RNA was obtained with TRIzol® Reagent (Invitrogen) following the manufacturer's indications. One milliliter of TRIzol was used per ten million cells. The isolated RNA was subsequently treated with RNase-free DNase (Promega) to remove any genomic DNA contamination.

Differential Display

mRNA differential display was carried out with the RNAimage kit (GenHunter, Nashville, TN) as previously shown (19). RNA from control astrocytes was compared with RNA obtained from astrocytes that had been subjected to OGD for 6 and 8 h. RNA bands with different intensity in controls and OGD-treated astrocytes were isolated, cloned, and sequenced. Sequence homology was analyzed using the BLASTnt alignment software.

Real-time Quantitative PCR (RT-PCR)

Changes in the mRNA expression were examined by RT-PCR using an ABIPrism 7000 Sequence Detection System (Applied Biosystems). cDNA (1 μl of reverse transcription product) was amplified using SYBR® Green PCR Master Mix (Applied Biosystems) in the presence of primer oligonucleotides specific for S6K1, Bcl-2, Bcl-xL, and GAPDH. The PCR

TABLE 1
Forward (FWD) and reverse (REV) primer sequences used to amplify the cDNAs of interest and the predicted product lengths

Name	Accession number	Sequence	Product size
			bp
S6K1	NM_001114334	FWD 5′-ATAGAATACATGGCCCCTGAA-3′ REV 5′-TGCTCCCAAACTCCACCAAT-3′	76
S6K2	NM_021485	FWD 5′-CGGGCTGAGAGGAACATTCTA-3′ REV 5′-CTGGAAAGCATAGGCCAGTTCT-3′	69
Bcl-2	NM_177410.2	FWD 5′-TGACTTCTCTCGTCGCTACCGT-3′ REV 5′-GGTGCAGCTGACTGGACATCTC-3′	55
Bcl-xL	X_83574.1	FWD 5′-AGAGGCAGGCGATGAGTTTGA-3′ REV 5′-AGATCACTGAACGCTCTCCGG-3′	50
GAPDH	BC083080	FWD 5′-GCCGGTGCTGAGTATGTCGT-3′ REV 5′-GCCTTCTCCATGGTGGTGAA-3′	56

conditions were as follows: 95 °C for 10 min, followed by 40 cycles consisting of 95 °C for 15 s and 60 °C for 1 min. Quantification was performed by the comparative C_t (cycle threshold) method (23), using the GAPDH expression level as internal control. Primers for all target sequences (Table 1) were designed using the computer Primer Express software provided with the 7000 Sequence Detection System (Applied Biosystems). Only one amplification product was obtained for each pair of primers, and its identity was confirmed by sequencing.

Preparation of Cell Extracts and Western Blotting

Astrocytes were scraped into ice-cold lysis buffer (50 mM Tris-HCl (pH 8), 120 mM NaCl, 2 mM sodium orthovanadate, 1% (v/v) Igepal, 15 mM sodium pyrophosphate, 1 mM benzamidine, 1 mg/ml pepstatin A, and Complete protease inhibitors (Roche Molecular Biochemicals). Cell debris was removed by centrifugation at 13,000 × *g* for 5 min, and the protein concentration was determined by the Bradford method. Cell lysates were loaded onto SDS-polyacrylamide gels, electrophoresed, and subsequently transferred to polyvinylidene fluoride membranes (Pall Corp., Ann Harbor, MI) as previously described (24). Membranes were probed with the anti-S6K1, anti-phosphoThr389 S6K, anti-S6K2, anti-phospoSer235/236 S6 anti-Bad, and anti-phosphoSer-136 Bad primary antibodies, and subsequently incubated with peroxidase-conjugated secondary antibodies following the manufacturer's instructions. An enhanced chemiluminescence system was used for visualization.

Immunoprecipitation

Immunoprecipitation was carried out on a rocking platform in a cold room. Astrocytes were harvested with lysis buffer containing 150 mM NaCl, 1% Nonidet P40, 0.5% sodium deoxycholate, 50 mM Tris (pH 7.5), 0.1 mM phenylmethylsulfonyl fluoride, 0.7 μg/ml leupeptin, and 0.5 μg/ml pepstatin. Total protein (0.5 mg) from each sample was precleared with 20 μl of protein A-agarose slurry (Roche Applied Science) for 3 h at 4 °C, and subsequently centrifuged at 12,000 × *g*. Supernatant was incubated overnight at 4 °C with 5 μg of Bad antibody. Protein A-Agarose (20 μl) was then added and incubated for 3 h. After centrifugation, the immunoprecipitate was washed twice with lysis buffer. Finally, sample loading buffer (20 μl) was added to the immunoprecipitate and boiled for 5 min before Western blot analysis.

Immunofluorescence Microscopy

Astrocytes grown on glass coverslips inserted in 6-well plates were washed twice with phosphate-buffered saline (PBS), fixed in 4% paraformaldehyde for 10 min at room temperature and blocked and permeabilized with 4% goat serum (Vector Laboratories, Burlingame, CA) plus 0.1% Triton X-100 in PBS. Cells were then incubated for 24 h at 4 °C with a rabbit anti-phospo-Ser-235/236 S6 antibody polyclonal antibody diluted 1:200 in PBS containing 4% goat serum. After subsequent washes with PBS, cells were incubated for 1 h at room temperature with a rhodamine (TRITC)-labeled goat anti-rabbit secondary antibody (Jackson Immunochemicals) diluted 1:5000. Fluorescent images of the cells were obtained with a Leica DMRXA microscope.

Viability Assays

MTT Assay—Cells were plated in 96-well culture plates at a density of 10,000 cells/well. At the indicated periods medium was removed and 100 μl of DMEM containing 0.5 mg/ml 3-[4,5-dimethylthiazol-2yl-2,5-diphenyltetrazolium bromide (MTT) was added. Cells were then incubated at 37 °C for 45 min in a CO_2 incubator. Finally, the MTT-containing medium was removed, and purple formazan crystals were dissolved by adding 100 μl of dimethyl sulfoxide to each well. Absorbance was measured in a microplate reader (Bio-Rad M-550) at 570 nm with a reference filter at 655 nm.

Fluorescence Microscope Imaging of Annexin V Staining—Astrocytes grown on coverslips were washed twice with PBS and stained for 15 min with Annexin V-Alexa Fluor 488 and propidium iodide (PI), according to the manufacturer's indications (Molecular Probes). Cells were then mounted on slides and observed under a fluorescence microscope using the appropriate filters.

Flow Cytometry for Annexin V/PI Assessment—Astrocytes were harvested by trypsinization and stained simultaneously with Annexin V-Alexa Fluor 488 and PI, according to the manufacturer's indications (Molecular Probes). Early apoptotic cells were distinguished from other cells with a BD-LSR flow cytometer (BD Biosciences). During apoptosis, phosphatidylserine is translocated from the inner to the outer leaflet of the plasma membrane, where it can be detected by Annexin V conjugates. Cells that were positive for Annexin V and negative for PI were considered early apoptotic. Annexin V-negative/PI-negative cells were identified as living cells, and cells positive for PI were designated as dead cells (necrotic plus late apoptotic cells).

Flow Cytometry for Intracellular ROS Production

Cells were incubated with the cell permeant dye H2DCF-DA, which de-esterifies intracellularly to H2DCF. ROS oxidize H2DCF to the brightly fluorescent compound 2′,7′-dichlorofluorescein, monitored by flow cytometry as previously described (24). Briefly, control and OGD-exposed astrocytes were incubated with 5 μM H2DCF-DA for 15 min at 37 °C, detached from the plate with trypsin/EDTA, resuspended in ice-cold PBS, and immediately used for flow cytometry. Triplicate samples were run in each experiment, and at

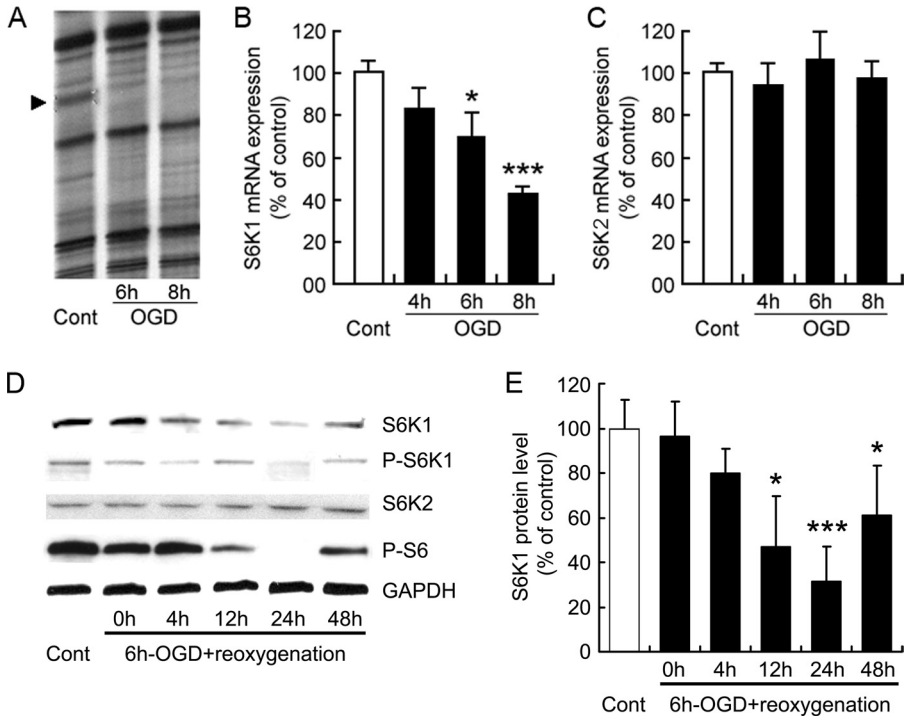

FIGURE 1. **OGD induces S6K down-regulation in astrocytes.** *A*, mRNA differential display gel corresponding to control (*Cont*) and 6- or 8-h OGD-treated astrocytes. The 258-bp band (*arrowhead*) down-regulated by OGD treatment showed 100% homology to the 3′ region of the mouse S6K1 gene. *B* and *C*, RNA samples obtained from controls and astrocytes exposed to OGD for 4, 6, and 8 h were used for quantification of S6K1 and S6K2 expression levels by reverse transcription followed by quantitative real-time PCR. GAPDH expression level was used as internal control. *D*, astrocytes were subjected to 6-h OGD, and total proteins were extracted immediately afterward or at different reoxygenation times (4, 12, 24, or 48 h). Control astrocyte cultures (*Cont*) were left untreated. Immunoblots were probed for S6K1, phospho-Thr-389 S6K1 (P-S6K), S6K2, phospo-Ser-235/236 S6 (P-S6), and GAPDH. A representative experiment is shown. *E*, S6K1/GAPDH ratio of signal intensity is shown. Immunoblot signals were quantified using the ImageJ software. Results (*B*, *C*, and *E*) are expressed as the mean ± S.D. of at least four experiments performed using independent astrocyte cultures. *, $p < 0.05$; ***, $p < 0.005$ relative to control.

least 10,000 cells per sample were analyzed. Mean fluorescence was calculated by using the program CellQuest.

Analysis of Protein Synthesis Rate

Protein synthesis rate was determined as described (25). Astrocytes, grown in 35-mm dishes were washed twice with cysteine- and methionine-free DMEM and incubated for 2 h in 1 ml of medium containing 40 μCi of [^{35}S]methionine and [^{35}S]cysteine (Amersham Biosciences). Cells were then washed twice in ice-cold PBS and lysed in 100 μl of 0.2% Triton. Three 10-μl aliquots from total cell lysate were counted in a scintillation counter to evaluate the label in total cell lysate. The remaining lysate was treated with trichloroacetic acid to precipitate proteins, and centrifuged at 12,000 × *g*. The amount of free radiolabel was assayed in three 10-μl supernatant aliquots in the scintillation counter. The amount of radiolabel incorporated into protein was then calculated by subtracting the value of the non-incorporated label from the value of the label in the total lysate.

Adenoviral Infection

Replication-defective adenoviral vectors driving the expression of Myc-tagged S6K1 (Ad-S6K1), kinase-dead S6K1 (Ad-KD-S6K1), and S6K2 (Ad-S6K2) were constructed as previously described (26). Adenoviruses were amplified in the permissive HEK-293 host cell line. Viral particles were purified by banding in a CsCl density gradient, and the viral titer was determined by the End-Point Dilution Assay as described before (19). Astrocytes were infected at a multiplicity of infection (m.o.i.) of 20 or 200, which resulted in a high transgene expression. An adenoviral vector expressing the β-galactosidase enzyme was used as control.

Statistics

All data were analyzed using the STATGRAPHICS plus 5.1 software package (Rockville, MD). Comparison between two groups was performed using Student's *t* test. One-way analysis of variance followed by a least significant differences test was applied when multiple comparisons were required. $p < 0.05$ was considered statistically significant.

RESULTS

OGD Induces S6K1 Down-regulation in Astrocytes—As an initial approach, experiments were set to search for genes involved in the response to ischemia in primary cultures of astrocytes. A strategy based in the RNA differential display technique was performed using OGD as a well established ischemia model. A consistent reduction of a 258-bp band was uncovered in OGD-treated astrocytes (Fig. 1*A*). This band, once isolated and sequenced, showed 100% homology to the 3′-end of the S6K1 mouse gene (accession number NM_001114334). Confirmatory quantitative RT-PCR experiments (Fig. 1*B*) revealed that S6K1 is abundantly expressed in control astrocytes and that S6K1 undergoes a prompt and prominent down-regulation following OGD (70 and 43% of control values after 6- and 8-h OGD, respectively). Conversely, the expression of the homologous gene S6K2 was not affected (Fig. 1*C*). Western blot analysis indicated that OGD-induced mRNA down-regulation is followed by a progressive reduction of S6K1 protein during the reoxygenation period, reaching the minimum values (31.43 ± 15.59%) at 24 h. Parallel reduction of the S6K1 phosphorylated active form and the phosphorylation of its target protein S6 were also observed. These values showed a partial recovery at 48 h after reoxygenation, although still persisted below controls (Fig. 1*D*). In contrast to S6K1, S6K2 levels were maintained during OGD and reoxygenation. Because ribosomal protein S6 is phosphorylated by both S6K1 and S6K2 in multiple tissues (25, 27–29), it is likely that OGD affects S6K1 and S6K2 enzymatic activity while specifically blunting S6K1 expression at the mRNA level.

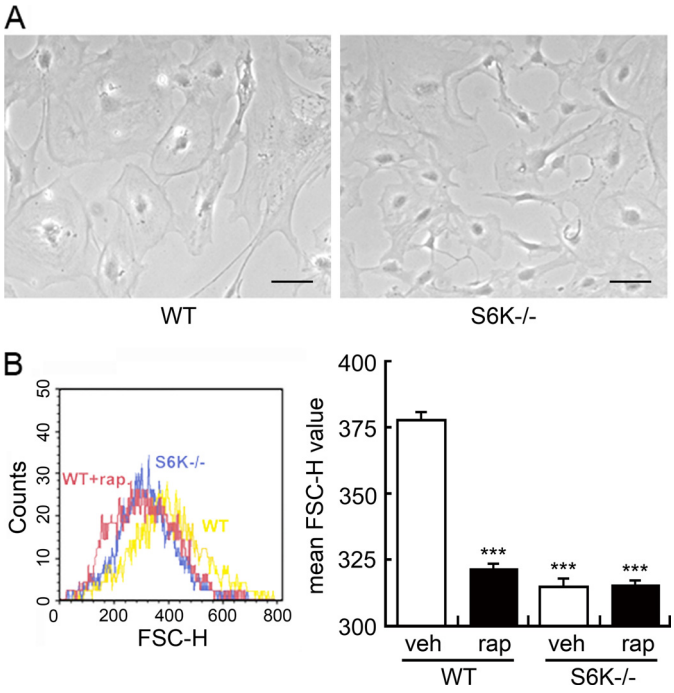

FIGURE 2. **S6K regulates astrocyte size.** *A*, representative phase-contrast microphotographs of primary astrocyte cultures from wild-type (WT) and S6K1;2$^{-/-}$ (*S6K*$^{-/-}$) animals. *Scale bars* correspond to 100 μm. *B*, both WT and S6K$^{-/-}$ cultures were exposed to 100 nM rapamycin (*rap*) or vehicle (*veh*) for 48 h. Astrocyte size was then analyzed by flow cytometry. Plot shows forward scatter height (*FSC*) values (*left panel*). Size measurements are presented as mean ± S.D. from five independent astrocyte cultures (*right panel*). ***, $p <$ 0.005 relative to untreated WT.

Regulation of Astrocyte Size by S6K—Our first approach to assess S6K function in astrocytes included preparation of primary astrocyte cultures obtained from S6K1;2$^{-/-}$ mice. These animals, developed by crossing S6K1$^{-/-}$ and S6K2$^{-/-}$ mice, had been previously reported to show reduced body weight and increased perinatal lethality (9). When astrocytes obtained from S6K1;2$^{-/-}$ mice were set in culture their proliferation rate was undistinguishable from wild-type astrocytes (not shown). However, astrocytes from S6K1;2$^{-/-}$ cultures displayed a 17% smaller size than wild-type counterparts (Fig. 2*A*), quantified by flow cytometry (Fig. 2*B*). Further assessment of the implication of S6K in cell size control was attained by pharmacological blockage of the mTOR/S6K pathway. Treatment of wild-type astrocytes with the mTOR inhibitor rapamycin greatly reduced astrocyte size, while the same treatment had no effect on S6K1;2$^{-/-}$ cells.

Protective Role of S6K on Astrocytes Exposed to Ischemia—In the next set of experiments we explored the consequences of S6K down-regulation in response to ischemia. In particular, we examined whether a lack in S6K activity could increase vulnerability of astrocytes to ischemic insults by comparing wild-type and S6K1;2$^{-/-}$ astrocyte cultures with respect to the effects of OGD on cell viability. Cultures were subjected to OGD for time intervals ranging from 0.5 to 16 h, and viability was assessed 24 h later by flow cytometry of Annexin V-PI staining (Fig. 3). S6K suppression significantly reduced astrocyte survival to ischemia, anticipating ischemia-induced death ~2 h. Highest differences in cell survival between wild-type and S6K1;2$^{-/-}$ astrocytes were obtained after 8-h OGD (56.56 ± 4.92% *versus* 38.36 ± 5.48%) (Fig. 3*A*). Moreover, quantification of Annexin V-positive/PI-negative cells (early apoptotic) indicated that increased cell death in S6K1;2$^{-/-}$ astrocytes exposed to either 4- or 8-h OGD also implicates a rise in apoptosis. Early apoptotic values for cells subjected to 4-h OGD are shown in Fig. 3, *B* and *C* (5.5 ± 0.49% for wild-type *versus* 8.07 ± 0.98 for S6K1;2$^{-/-}$ astrocytes). These *panels* also show that the number of PI-positive cells (late apoptotic and necrotic) is higher in S6K1;2$^{-/-}$ (27.24 ± 4.34) than in wild-type astrocyte cultures (18.36 ± 2.58%); suggesting that, besides apoptosis, necrotic death pathways are involved in the increased susceptibility of S6K1;2$^{-/-}$ astrocytes to OGD. These findings were further confirmed by fluorescence microscopy examination of Annexin V- and PI-stained cells (Fig. 3*D*).

Complementary data on the beneficial role of the mTOR/S6K pathway on astrocyte viability were obtained analyzing the effects of mTOR inhibition. Astrocytes obtained from wild-type mice were serum-starved for 24 h and pretreated with rapamycin for 24 h prior to 4-h OGD. Viability was assessed after 24-h reoxygenation by flow cytometry of Annexin V-PI-stained cells. The results obtained showed that rapamycin significantly increased OGD-induced astrocyte injury. Values for both early apoptotic and late apoptotic/necrotic cells were raised by rapamycin (8.6 ± 1.2 and 14.6 ± 2.5% in vehicle-*versus* 10.5 ± 0.8 and 22.4 ± 4.7% in rapamycin-treated astrocytes), while the percentage of live cells was reduced from 75.7 ± 5.8 to 61.4 ± 3.5% (Fig. 4). Therefore, these experiments support the notion that S6K activation by mTOR preserves astrocytes from ischemic damage.

Astrocyte Protection against OGD Depends on S6K1, but Not S6K2—To address whether S6K1 or S6K2 were responsible for the protective functions, astrocytes obtained from S6K1;2$^{-/-}$ mice were infected with adenoviral vectors expressing either Myc-tagged S6K1 or S6K2 (Adeno-S6K1 and Adeno-S6K2, respectively). Infection of cells with both forms of the S6K adenovirus resulted in comparable levels of expression, as determined by Western blot analysis with anti-Myc antibody. S6K1 levels obtained with Adeno-S6K1 at m.o.i. 20 were similar to the endogenous protein levels observed in wild-type astrocytes, whereas 200 m.o.i. induced much higher levels (Fig. 5*B*). As expected, ribosomal protein S6 phosphorylation was absent in S6K1;2$^{-/-}$ cultures infected with β-galactosidase-expressing adenovirus (Adeno-β-gal). Expression of either S6K1 or S6K2 induced the phosphorylation of ribosomal protein S6 in astrocytes (Fig. 5, *A* and *B*), indicating that both kinases can rescue ribosomal protein S6 phosphorylation. To compare the protective roles of S6K1 and S6K2, S6K1;2$^{-/-}$ astrocytes were infected with Adeno-β-gal, Adeno-S6K1, or Adeno-S6K2 at the indicated m.o.i. and then subjected to 6-h OGD. Twenty-four hours later, cell viability was analyzed by the MTT reduction assay. Results show that S6K1 expression increases astrocyte survival to OGD, whereas S6K2 is ineffective. Moreover, astrocyte transduction with an adenoviral vector driving the expression of inactive S6K1 (KD-S6K1) did not improve astrocyte survival to OGD (Fig. 5*D*). Hence, our results indicate that S6K protection against astrocyte ischemia resides specifically on S6K1 activity.

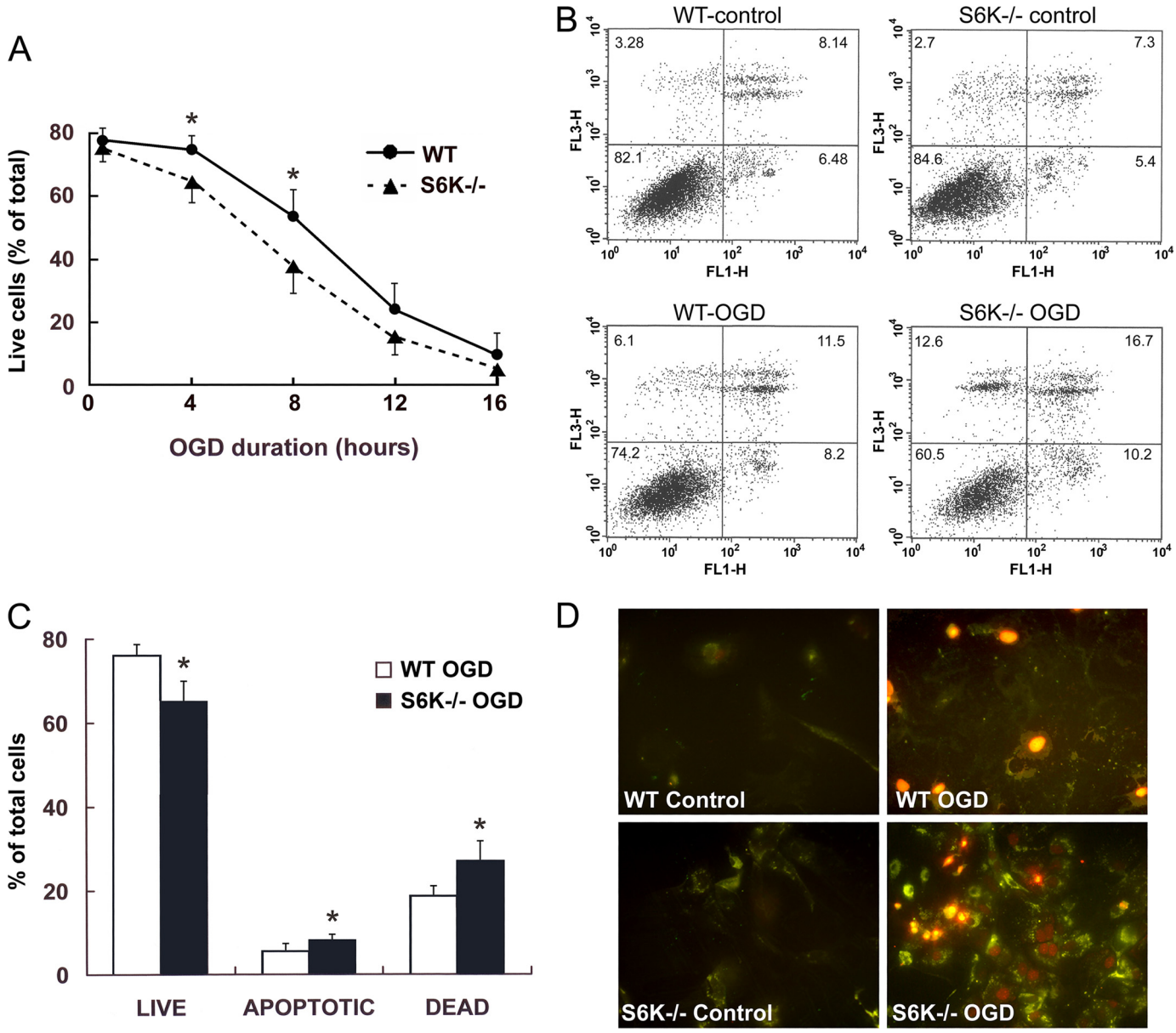

FIGURE 3. **S6K1;2$^{-/-}$ astrocytes show increased susceptibility to ischemic damage.** Astrocytes derived from either S6K1;2$^{-/-}$ or WT mice were subjected to OGD for the indicated times, and cell viability was analyzed by Annexin V-PI staining followed by flow cytometry or fluorescence microscopy 24 h after the OGD onset. *A*, time course of ischemia-induced astrocyte death. WT and S6K1;2$^{-/-}$ astrocyte cultures were exposed to OGD for 0.5, 4, 8, 12, or 16 h, and cell viability was assessed by flow cytometry. Values represent the percentage of viable cells (PI-negative/Annexin V-negative). *B*, representative flow cytometry analysis of Annexin V-PI staining in control and 4-h OGD-treated WT and S6K1;2$^{-/-}$ astrocytes. PI fluorescence was plotted *versus* Annexin V-Alexa Fluor 488 fluorescence. Cells located in the *lower right quadrant* (PI-negative/Annexin V-positive) were designated early apoptotic. Cells in the *lower left quadrant* (PI-negative/Annexin V-negative) were considered viable, and cells in the *upper quadrants* (PI-positive) were considered late apoptotic or necrotic. *C*, quantitative analysis of flow cytometry results corresponding to 4-h OGD-treated WT and S6K1;2$^{-/-}$ astrocytes. *D*, representative micrographs of all experimental groups described in *panel B*. *Green* staining indicates Annexin V-Alexa Fluor 488 binding to the exposed phosphatidylserine tails, whereas *red color* corresponds to PI nuclear staining. Values in *A* and *C* are expressed as percentage of the total number of cells counted in each culture and represent the mean ± S.D. of at least four independent experiments. *Asterisks* denote significant differences between WT and S6K1;2$^{-/-}$ astrocytes (*, $p < 0.05$).

S6K Suppression Modifies the Balance between Pro- and Anti-apoptotic Factors—Among the putative S6K substrates, the proapoptotic protein BAD has been shown to be phosphorylated at Ser-136 and inactivated by S6K1 after insulin-like growth factor stimulation (14). To check whether this pro-apoptotic factor was related to the increased death observed in OGD-exposed S6K1;2$^{-/-}$ astrocytes, we analyzed the levels of phospho-Ser-136-BAD by immunoprecipitation and Western blotting. Protein extracts were obtained from wild-type and S6K1;2$^{-/-}$ astrocytes exposed to 4-h OGD followed by 24-h reoxygenation. The results obtained demonstrate that BAD phosphorylation at Ser-136 is intensely impaired in S6K1;2$^{-/-}$ astrocytes (Fig. 6*A*), also suggesting that S6K induces the inactivation of BAD by phosphorylation during ischemia. However, the fact that BAD phosphorylation was diminished in S6K1;2$^{-/-}$ astrocytes, but not absent, implicates that additional kinases contribute to the inactivation of this proapoptotic factor.

The effect of S6K suppression on the pro-apoptotic factor BAD prompted us to determine if other Bcl-family members,

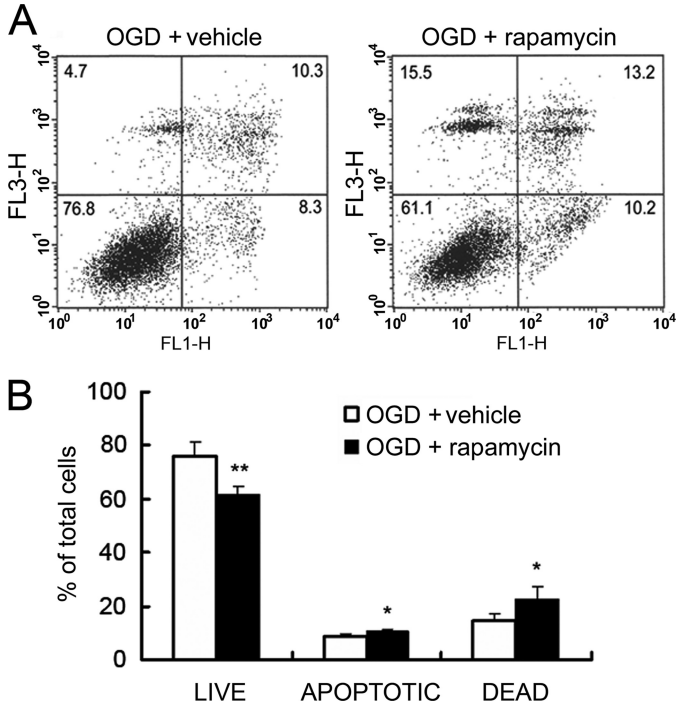

FIGURE 4. **Rapamycin increases astrocyte damage induced by OGD.** Astrocytes pretreated for 24 h with 100 nM rapamycin or vehicle were subjected to 4-h OGD followed by a 24-h reoxygenation period. Cell viability was then assayed by flow cytometry. *A*, representative plots of PI *versus* Annexin V-Alexa Fluor 488 fluorescence intensity corresponding to both vehicle- and rapamycin-treated astrocytes. *B*, quantitative analysis of flow cytometry results expressed as percentage of total number of cells counted. Values represent the mean ± S.D. of at least four independent experiments. *Asterisks* show significant differences between vehicle- and rapamycin-treated astrocytes within the live, apoptotic, or dead cell group (*, $p < 0.05$; **, $p < 0.01$).

such as Bcl-2 and Bcl-xL, were also regulated by S6K. Measuring Bcl-2 and Bcl-xL expression levels by RT-PCR revealed that both anti-apoptotic factors are significantly decreased in S6K1;2$^{-/-}$ after OGD in comparison to wild-type astrocytes (Fig. 6*B*). Differences were more dramatic for Bcl-xL, because OGD enhanced its expression in wild-type astrocytes while inducing down-regulation in the S6K1;2$^{-/-}$ group. Interestingly, no differences in Bcl-2 and Bcl-xL mRNA expression or BAD phosphorylation were observed in the absence of OGD (not shown). In conclusion, our experiments underscore the essential role of S6K to maintain an adequate proapoptotic/anti-apoptotic balance in astrocytes exposed to OGD. Furthermore, these observations suggest that S6K1;2$^{-/-}$ regulates pro- and anti-apoptotic factors in astrocytes in the context of energy deprivation rather than in resting conditions.

S6K Regulates ROS Levels in Astrocytes—ROS generation is a common cellular mechanism for multiple death pathways. To investigate whether ROS are involved in the effects of S6K on astroglial viability, ROS production was evaluated in H2DCF-loaded astrocytes by flow cytometry (Fig. 7*A*). S6K1;2$^{-/-}$ astrocytes showed significantly higher basal ROS levels (150% relative to wild-type astrocytes). Moreover, OGD induced a sharp increase in ROS levels in wild-type astrocytes (280%), which was even more prominent in S6K1;2$^{-/-}$ cells (525%). These experiments indicate that S6K down-regulation is associated to ROS production, and that ROS levels correlate with the amount of astrocyte death observed in wild-type and S6K1;2$^{-/-}$ astrocytes.

Next step was to test whether ROS generation is involved in the reduction of cell viability observed in S6K1;2$^{-/-}$ astrocytes following OGD exposure. In these experiments we used the antioxidant *N*-acetyl-L-cysteine, which provides cysteine for GSH synthesis and spares GSH by reacting with ROS. Primary astrocytes from both wild-type and S6K1;2$^{-/-}$ animals were pretreated for 24 h with *N*-acetyl-L-cysteine (1 mM, Fig. 7*B*) before being challenged with 4-h OGD. Cell viability, assessed 24 h later by the MTT reduction assay, revealed that this antioxidant treatment abolished OGD-induced cytotoxicity in S6K1;2$^{-/-}$ astrocytes as much as in wild-type cells. Therefore, these experiments identify ROS as an essential component of the apoptotic pathway regulated by S6K in astroglial cells.

Our previous analysis suggests that S6K moderates ROS production in oxidative conditions such as OGD. If this is the case, S6K1;2$^{-/-}$ astrocytes should display increased susceptibility to other oxidants as well. We tested this hypothesis by using hydrogen peroxide (H_2O_2) and 6-hydroxydopamine, two drugs widely used to induce oxidative stress in astrocytes. Comparison of their effects on the viability of wild-type and S6K1;2$^{-/-}$ astrocytes revealed that treatment with both H_2O_2 and 6-hydroxydopamine induces significantly more injury in S6K1;2$^{-/-}$ astrocytes than in wild-type cells (Fig. 7, *C* and *D*).

S6K1 and S6K2 overexpression experiments were performed to determine which of the kinases is involved in ROS regulation. Our results indicate that S6K1 expression, but not S6K2, significantly reduces ROS levels in astrocytes exposed to OGD (Fig. 7*E*). Taken together, our results suggest that S6K1 is required for astrocytes to cope with oxidative stress and to confer protection against OGD.

Protein Synthesis Recovery after OGD Is Impaired in S6K1;2$^{-/-}$ Astrocytes—Translational arrest is observed in "*in vivo*" models of both global and focal cerebral ischemia where it shows a striking correlation with neuronal vulnerability (16, 30, 31). Thus we have measured translation rate by analyzing the incorporation of [^{35}S]methionine and [^{35}S]cysteine to astrocytes at different reoxygenation times after OGD. According to these experiments (Fig. 8), OGD causes a decrease in the rate of protein synthesis significantly more prominent in S6K1;2$^{-/-}$ than in wild-type astrocytes after a 24-h reoxygenation period. Moreover, although the translational rate in wild-type astrocytes has largely recovered 72 h after reoxygenation started (89%), no recuperation was observed in S6K1;2$^{-/-}$ astrocytes (40%). Contrarily, in the absence of OGD no differences were observed in protein synthesis between wild-type and S6K1;2$^{-/-}$ astrocytes. Differences in protein synthesis recovery cannot be attributed to an increase in the number of viable cells between 24- and 72-h reoxygenation, because cell survival did not significantly increase in either wild-type or S6K$^{-/-}$ astrocytes during this period (not shown). Because the absence of S6K has a strong impact on translation, these observations confirm that S6K play key roles in astrocytes to maintain cellular functions under ischemia.

S6K Suppression Increases Ischemic Damage in an in Vivo Model of Ischemia—Our experiments have shown protective effects of S6K1 in astrocytes using an *in vitro* model of ischemia.

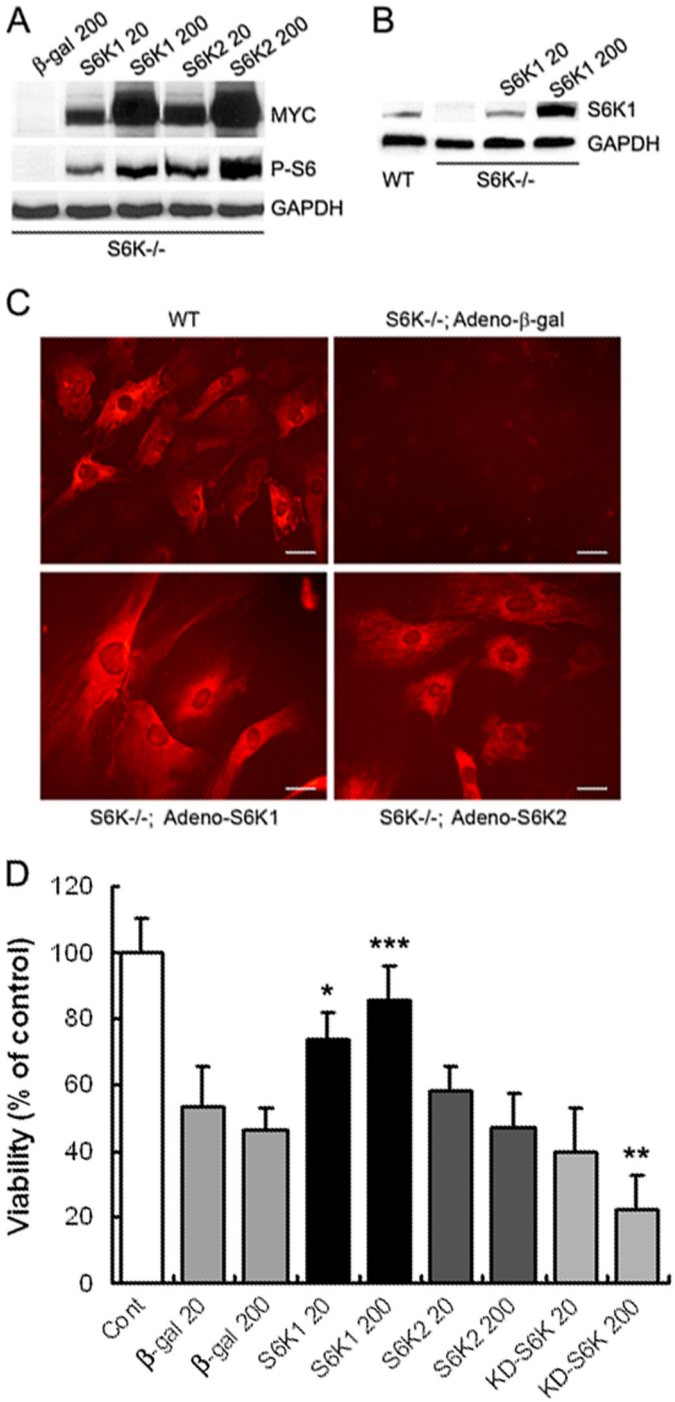

FIGURE 5. **S6K1, unlike S6K2, protects astrocytes against OGD.** Expression of exogenous S6K1, S6K2, or kinase-dead S6K1 (*KD-S6K*) was achieved by an adenoviral system. *A*, S6K1;2$^{-/-}$ astrocyte cultures were transduced with Myc-tagged S6K1 or S6K2 or β-galactosidase (*β-gal*) adenovirus at the indicated m.o.i. (20 or 200). Transduction efficiency was assessed by Western blot analysis with anti-Myc or anti-phospo-Ser-235/236 S6 antibodies to assess S6K activity. *B*, comparison of S6K1 protein levels obtained by adenoviral transduction of S6K1;2$^{-/-}$ astrocytes (*S6K1 20* and *S6K1 200*) to the endogenous levels found in wild-type cells. *C*, immunofluorescence microscopy analysis of wild-type (*WT*) and S6K1;2$^{-/-}$ astrocyte cultures transduced with adenovirus expressing S6K1, S6K2, or β-galactosidase (*β-gal*). All cells were stained with anti-phospo-Ser-235/236 S6 antibodies to detect S6K activity. *Scale bars* correspond to 100 μm. *D*, S6K1;2$^{-/-}$ astrocytes infected with β-gal-, S6K1-, S6K2, or KD-S6K-expressing adenoviral vectors at the indicated m.o.i. were subjected to 6-h OGD. Viability was measured after a 24-h reoxygenation period by the MTT reduction method. Results represent the mean ± S.D. of 4–6 independent experiments, and are expressed as percentage of uninfected S6K1;2$^{-/-}$ controls not exposed to OGD. *, $p < 0.05$; ***, $p < 0.005$, relative to β-gal-expressing cells.

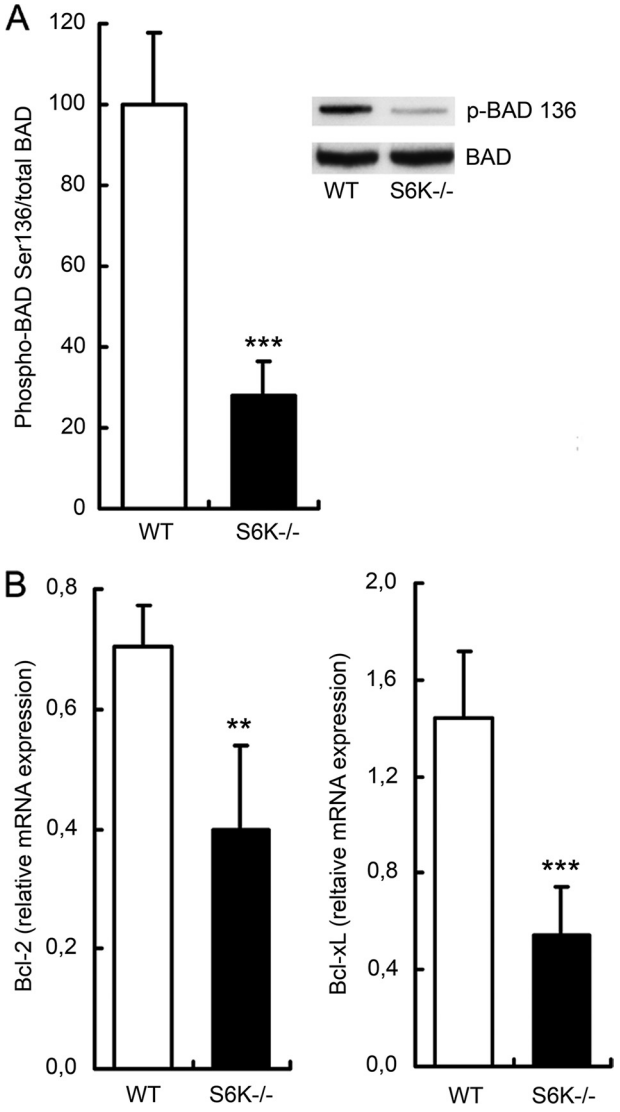

FIGURE 6. **S6K suppression impairs BAD phosphorylation and decreases Bcl-2 and Bcl-xL expression.** Astrocytes derived from either S6K1;2$^{-/-}$ or wild-type mice were subjected to 4-h OGD followed by a 24-h reoxygenation period, and total protein or RNA was extracted. *A*, BAD phosphorylation at Ser-136 was analyzed by immunoprecipitation, and immunoblots were probed for BAD and phospo-Ser-136 BAD. *Histograms* show results as percentage of OGD-exposed WT astrocytes. A representative experiment is shown in the inset. *B*, Bcl-2 and Bcl-xL mRNA expression levels were analyzed by quantitative real-time PCR. GAPDH expression level was used as internal control. Numeric values are presented as percentage of WT astrocytes not exposed to OGD. Results are expressed as mean ± S.D. of at least three independent experiments in both panels (**, $p < 0.01$, relative to OGD-treated WT astrocytes).

To validate *in vivo* the roles assigned to S6K, permanent MCAO was performed on both wild-type and S6K1;2$^{-/-}$ mice, as an animal model of ischemic stroke. The consequences of S6K suppression on animal survival were then analyzed. We found that S6K-deficient mice were more prone to die than wild-type littermates during the 8-day period of study (Fig. 9*A*).

Although infarct volume was similar 48 h after MCAO induction, at 7 days it was significantly higher in S6K1;2$^{-/-}$

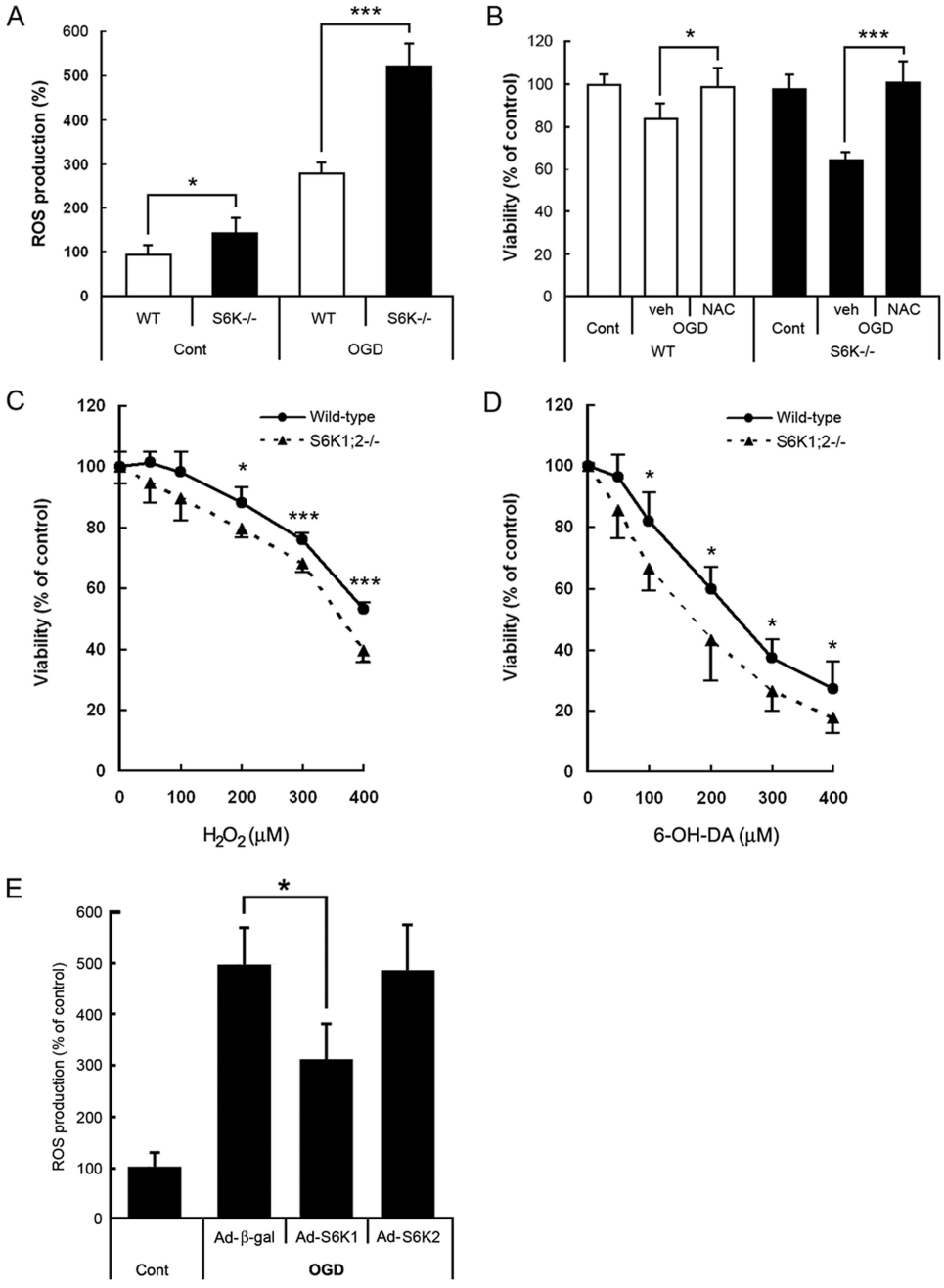

FIGURE 7. **ROS accumulation in S6K1;2$^{-/-}$ astrocytes contributes to OGD-induced apoptosis and renders astrocytes more sensitive to oxidative stress.** *A*, astrocytes derived from either S6K1;2$^{-/-}$ or wild-type mice were subjected to 6-h OGD followed by 1-h reoxygenation. ROS levels were analyzed afterward by flow cytometry using the ROS-sensitive dye DCF. Results are presented as percentage of untreated wild-type values. *B*, astrocyte cultures from wild-type or S6K1;2$^{-/-}$ mice were pretreated for 24 h with the antioxidant *N*-acetyl-L-cysteine (1 mM) or vehicle and subjected to 4-h OGD. Cell viability was analyzed 24 h later by the MTT reduction assay. *C* and *D*, wild-type or S6K1;2$^{-/-}$ astrocytes were treated with H_2O_2 or 6-hydroxydopamine at the indicated concentrations for 24 h, and cell viability was assessed by the MTT method. *E*, S6K1;2$^{-/-}$ astrocytes were transduced with the indicated adenoviral vectors at a m.o.i. of 20 and 24 h later subjected to 6-h OGD. ROS levels were analyzed after 1-h reoxygenation. Results are expressed as percentage of uninfected S6K1;2$^{-/-}$ controls not exposed to OGD. *, $p < 0.05$; relative to β-galactosidase-expressing cells. Results in *all panels* represent mean ± S.D. of at least four independent experiments. *, $p < 0.05$; ***, $p < 0.005$.

mice (25.93 ± 3.29 mm^3/100 mg of tissue) than in wild-type animals (16.60 ± 2.51 mm^3/100 mg of tissue). It is also interesting to note that, although a significant decrease on infarct size was observed between days 2 and 7 following MCAO in wild-type mice, this reduction was completely absent in S6K-deficient animals; in which infarct size showed the opposite trend (Fig. 9*B*). In summary, because mortality and cerebral infarct volume were increased in mutant mice, the results obtained from our *in vivo* model of brain stroke suggest that S6K plays a protective role.

DISCUSSION

By using mouse lacking S6K activity, we have shown for the first time that S6K1 is required for protection against ROS, protein synthesis and astrocyte survival after oxygen and glucose deprivation. Moreover S6K activity limits brain damage induced by middle cerebral artery occlusion, an *in vivo* model of ischemia. Since we and others have shown that the mTOR/S6K pathway is regulated by oxygen and glucose levels, our functional studies define an important signal transduction element for astroglial function during ischemic conditions.

A differential display mRNA assay to search for genes involved in the astrocyte response to ischemia led to the first evidence that S6K1 is down-regulated in these cells in response to OGD. This initial strategy to show a reduction in S6K1 mRNA was later complemented with experiments that evidenced a significant diminution in total S6K peptide as well as a profound decline of its active, phosphorylated form. Consistent with the S6K inactivation, phosphorylation of its target, the ribosomal S6 protein, a component of the translation machinery, was also decreased by OGD in astrocytes. In agreement with our data, previous reports have shown dephosphorylation and down-regulation of S6K as a consequence of focal and global brain ischemia *in vivo* (15–17, 32). Therefore, there is enough evidence to sustain that S6K inactivation may have important consequences for functional recovery. In addition, our work supports the notion that S6K also displays prosurvival functions based on the regulation of pro- and anti-apoptotic factors in conditions of cellular stress such as ischemia. This emerging mechanism of protection by S6K would accompany the well known effects of the kinase on cell growth.

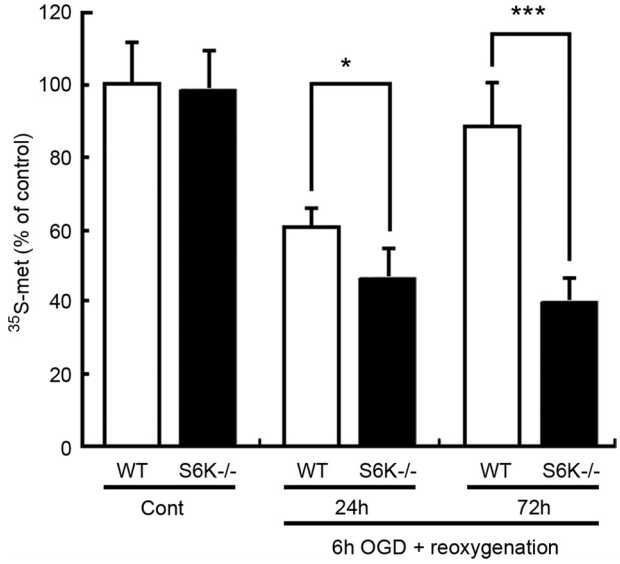

FIGURE 8. **S6K suppression impairs protein synthesis recovery after OGD.** Astrocytes derived from either S6K1;2$^{-/-}$ or wild-type mice were subjected to 6-h OGD followed by reoxygenation for 24 or 72 h. The rate of protein synthesis was then determined by measuring incorporation of [^{35}S]methionine and [^{35}S]cysteine into cellular proteins. Values represent mean ± S.D. of three independent experiments. Results are expressed as percentage of WT controls not subjected to OGD. *, $p < 0.05$; ***, $p < 0.005$.

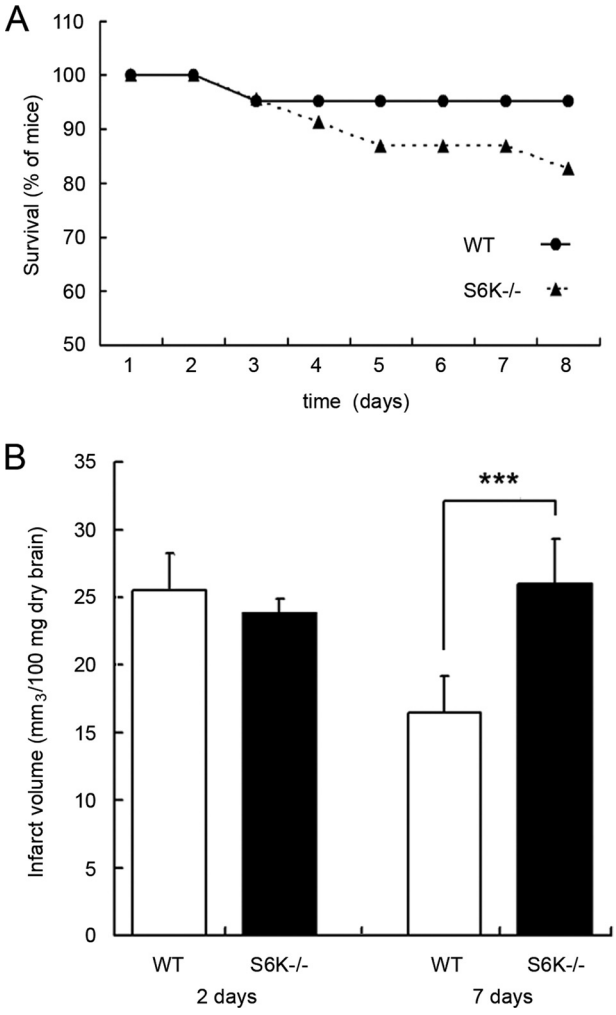

FIGURE 9. **S6K suppression increases mortality and infarct volume after focal ischemia.** MCAO was performed in WT and S6K1;2$^{-/-}$ mice. *A*, percentage of mice survival is shown. *B*, infarct volume was measured at 2 and 7 days after MACO. Results show the infarct volume (in mm^3 per 100 mg of dry tissue) and represent the mean ± standard deviation of 4–5 mice. ***, $p < 0.005$.

As previously shown in other cell types, astrocyte cell size depends on S6K activity. Our strategy to ascertain S6K functions on astrocyte exposed to ischemia involved the use of knock-out mice in which both forms of S6K (S6K1 and S6K2) had been suppressed by homologous recombination. Previous studies illustrated that simultaneous deletion of S6K1 and S6K2 provides a significant increase in perinatal lethality as well as a small size phenotype (9). In turn, deletion of only S6K1 provides a small mice phenotype with reduction of pancreatic β-cells (33) and myoblast size (28); whereas S6K2 mutants are normal. Thus, our data showing that S6K1;2$^{-/-}$ astrocytes are smaller than wild-type counterparts are in agreement with earlier work and support the role of this kinase as a master regulator of cell growth. Differences in astrocyte size were marked, because they were clearly visible under the microscope. Moreover, quantification by flow cytometry revealed that S6K suppression causes a 17% reduction in astrocyte size, which is a similar change to those described for pancreatic β-cells (33) and myoblasts (28). We further confirmed that the phosphorylated-active form of S6K is necessary for astrocyte growth using rapamycin. The result of this treatment, a 15% size reduction of wild-type astrocytes and no effect on S6K1;2$^{-/-}$ astrocytes, is again in agreement with previous reports on pancreatic β-cells and myoblasts.

In addition to these growth promoting effects, the use of S6K1;2$^{-/-}$ mice in combination with an *in vitro* model of ischemia was essential to unmask the protective role of S6K on astrocytes. S6K suppression in S6K1;2$^{-/-}$ mice greatly increased astrocyte injury caused by OGD, shifting the OGD duration/viability curve approximately 2 h to the left. It could also be inferred that astrocyte death caused by OGD in S6K1;2$^{-/-}$ astrocytes was due, at least partially, to increased apoptosis, as the number of Annexin V positive cells was significantly higher in S6K1;2$^{-/-}$ than in wild-type astrocytes. In a confirmatory set of experiments, mTOR inhibition by rapamycin significantly increased death of wild-type astrocytes only when exposed to OGD. Besides demonstrating that S6K is protective for astrocytes, these results show that the protective function against ischemia resides in phosphorylated/active S6K. The second conclusion that can be drawn is that S6K is specifically involved in the response to stress conditions, whereas unstressed astrocytes can support mTOR inhibition without any loss of viability. It should also be pointed out that these findings could be relevant for patients treated with rapamycin, because there is a chance that this drug worsens the prognosis of brain pathologies associated to astrocyte apoptosis.

We analyzed the levels of phosphorylation of the proapoptotic factor BAD in a first attempt to elucidate the mechanism by which S6K confers protection. BAD was elected, because it meets the most stringent criteria as an S6K substrate (34). Besides, it has been linked to S6K protective functions before. Thus, S6K was demonstrated to mediate insulin-like growth factor 1 protective functions by inactivating BAD by phosphorylation at Ser-136, ultimately leading to its interaction with

14-3-3 proteins and degradation (14). Our results showing that BAD phosphorylation at Ser-136 is prominently impaired in S6K1;2$^{-/-}$ astrocytes indicates that S6K is also necessary for BAD inactivation in these cells. Moreover, we present experiments that illustrate that the increased apoptosis observed in OGD-exposed S6K1;2$^{-/-}$ astrocytes correlates with deficient BAD phosphorylation by S6K. These results are in agreement with a previous report linking BAD function and ischemia in astrocytes, because BAD inactivation was shown to dramatically increase survival after ischemia (35). In the same line, the protective role of insulin in cardiac ischemia also seems to implicate S6K-dependent BAD phosphorylation at Ser-136 (18).

In addition to BAD hypophosphorylation, our results indicate that exposure of S6K1;2$^{-/-}$ astrocytes to OGD induces the down-regulation of survival factors such as Bcl-2 and Bcl-xL. Therefore, it could be suggested that S6K, possibly acting through multiple pathways, arbitrates the equilibrium between intracellular pro- and anti-apoptotic factors. Further expanding the possible attributions of S6K, an array of new substrates of S6K has recently been identified (34). These considerations, together with the fact that both S6K1 and S6K2 have nuclear localization signals, lead to the challenging hypothesis that S6K might regulate the expression of Bcl-2, Bcl-xL or other targets at the transcriptional level, acting in the nucleus by direct phosphorylation of transcriptional regulators.

Interestingly we find that this unbalance between pro- and anti-apoptotic factors in S6K1;2$^{-/-}$ astrocytes is accompanied by increased ROS accumulation in response to OGD. Further evidence indicating that elevated ROS levels are linked to increased susceptibility to OGD were obtained with the use of antioxidants, because *N*-acetyl-L-cysteine pretreatment completely avoided OGD-induced S6K1;2$^{-/-}$ astrocyte death. It is well established that mitochondrial impairment during stress is associated with the generation of ROS. These, in turn, induce cell damage through the oxidation of proteins, lipids, and DNA. Because recent studies suggest that not only neurons but also astrocytes may experience mitochondrial dysfunction during ischemia-reperfusion (36–38), it is tempting to speculate that the protective role of S6K on astrocytes involves the preservation of mitochondrial integrity during ischemia. In line with this postulation, the tumor suppressor phosphatase and tensin homolog, which inhibits the phosphatidylinositol 3-kinase/mTOR/S6K pathway (39), increases ROS in *in vitro* models of stroke and Parkinson disease (40). Moreover, our model of S6K deletion renders astrocytes more susceptible not only to OGD, but also to H_2O_2 and 6-hydroxydopamine-induced toxicity; which is in consonance with the implication of S6K in possible defense mechanisms against oxidative stress.

We have shown that enhanced apoptosis of astrocyte in S6K-null mice is associated with increased ROS production, whose source would be damaged mitochondria. Given that Bcl-2 family members, shown here as targets of S6K, are key regulators of the mitochondrial pathway of apoptosis, it could be suggested that the mitochondrial dysfunction caused by S6K down-regulation may be a consequence of an unbalance between pro- and anti-apoptotic Bcl-2 family members. However, other mechanisms may also operate, because a recent study in cardiac myocytes has described an alternative pathway by which S6K affects mitochondrial ROS release acting on the permeability transition pore complex through the inhibition of glycogen synthase kinase 3β (41).

Astrocytes are a central component of the brain's antioxidant defense (42, 43), and their ability to maintain antioxidant functions may be a critical determinant of neuronal survival and brain function after ischemia. Therefore, even though the study of astrocyte-neuron interactions is beyond the scope of this article, it is important to consider that the regulation of S6K activity in astrocytes may have obvious implications for neuronal integrity.

Historically S6K has been recognized as a master regulator of translation, a role mediated by the phosphorylation of its classic target protein, the ribosomal protein S6. However, several controversial reports claim that not only 5′ terminal oligopyrimidine tract mRNA translation, but also the overall transcriptional rate, are not depressed in S6K mutant mice (9, 25, 44). In accordance with these observations, our experiments aimed to assess the degree of S6K implication in astrocyte protein synthesis following OGD showed that wild-type and S6K1;2$^{-/-}$ astrocytes do not differ in protein synthesis rate. Therefore, it can be conceived that S6K is not essential for protein synthesis under control conditions. On the contrary, profound differences were observed between wild-type and S6K-null astrocytes when protein synthesis rates were measured after ischemia. 72 h after OGD, translation had significantly recovered in wild-type cells but continued deeply impaired in mutant astrocytes. In conclusion, our results support the notion that S6K may be a critical checkpoint in the path to resume protein synthesis and facilitate functional recovery after brain ischemia, but is not a critical player in the regulation of astrocytic basal translation.

It is well established that S6K1 and S6K2, besides being highly homologous, share the ability to respond to common activating pathways and, to phosphorylate S6 (45). Here we confirm that both S6K1 and S6K2 are capable to rescue rpS6 phosphorylation in S6K1;2$^{-/-}$ astrocytes. On the other hand, the same set of experiments highlights the idea that these kinases differ in a number of cellular functions, because only S6K1 was able to provide resistance to OGD-lowering ROS levels. In accordance with these observations, recent reports have revealed that not all the substrates of S6K1 or S6K2 are common. As an example, SKAR, implicated in cell size regulation, has been identified as a S6K1 substrate but is not phosphorylated by S6K2 (46). In the same line, although both kinases have shown cell survival functions, the pathways implicated differed. Although S6K1 was associated to BAD inactivation (14, 18), S6K2 was observed to mediate survival by forming a mitogen-stimulated complex with B-Raf and protein kinase C epsilon (47).

Finally, we were able to validate *in vivo* our previous observations by assessing the role of S6K in a well established brain ischemia model consisting on the permanent occlusion of the middle cerebral artery. In agreement with the protective role of S6K shown in astrocyte cultures, stroke-related mortality of mice was higher in S6K1;2$^{-/-}$ animals than in wild-type counterparts. In addition, striking differences emerged in infarct volume 7 days after occlusion, because infarct volume was significantly reduced in wild-type mice while no signs of improve-

ment were observed in S6K-null mice. Strikingly, 48 h after ischemia both mice were undistinguishable in terms of infarct volume, indicating that the protective functions of S6K are only evident at later stages of brain infarct. Consequently, key questions on the underlying mechanisms are still unresolved, and future experiments will be required to obtain a better understanding of S6K control on infarct evolution. Whether or not astrocyte function impairment accounts for the increased infarct size and ischemia-related mortality observed in S6K1; $2^{-/-}$ mice subjected to permanent *in vivo* ischemia awaits for clarification.

Taken together, our results illustrate that astrocytes obtained from S6K1;$2^{-/-}$ mice are more susceptible to *in vitro* ischemia than wild-type cells. Evidence gathered also indicate that the increased damage in S6K1;$2^{-/-}$ astrocytes is the consequence of a combination of deficiencies that include a reduction in protein synthesis and BAD phosphorylation and alterations in ROS management in response to OGD. Therefore, the different animal and cellular models presented here emphasize the notion that S6K plays a significant protective role against brain damage caused by ischemia and that astrocytes are direct beneficiaries of S6K protection.

Acknowledgments—We thank Gema Rodriguez, Estefanía Chantre, Isabel Sevilla, and Vanesa Guijarro for their expert technical assistance.

REFERENCES

1. Li, L., Lundkvist, A., Andersson, D., Wilhelmsson, U., Nagai, N., Pardo, A. C., Nodin, C., Ståhlberg, A., Aprico, K., Larsson, K., Yabe, T., Moons, L., Fotheringham, A., Davies, I., Carmeliet, P., Schwartz, J. P., Pekna, M., Kubista, M., Blomstrand, F., Maragakis, N., Nilsson, M., and Pekny, M. (2008) *J. Cereb. Blood Flow Metab.* **28,** 468–481
2. Wullschleger, S., Loewith, R., and Hall, M. N. (2006) *Cell* **124,** 471–484
3. Brugarolas, J., Lei, K., Hurley, R. L., Manning, B. D., Reiling, J. H., Hafen, E., Witters, L. A., Ellisen, L. W., and Kaelin, W. G., Jr. (2004) *Genes Dev.* **18,** 2893–2904
4. Inoki, K., Zhu, T., and Guan, K. L. (2003) *Cell* **115,** 577–590
5. Reiling, J. H., and Hafen, E. (2004) *Genes Dev.* **18,** 2879–2892
6. Manning, B. D., and Cantley, L. C. (2003) *Biochem. Soc. Trans.* **31,** 573–578
7. Holz, M. K., Ballif, B. A., Gygi, S. P., and Blenis, J. (2005) *Cell* **123,** 569–580
8. Gingras, A. C., Raught, B., Gygi, S. P., Niedzwiecka, A., Miron, M., Burley, S. K., Polakiewicz, R. D., Wyslouch-Cieszynska, A., Aebersold, R., and Sonenberg, N. (2001) *Genes Dev.* **15,** 2852–2864
9. Pende, M., Um, S. H., Mieulet, V., Sticker, M., Goss, V. L., Mestan, J., Mueller, M., Fumagalli, S., Kozma, S. C., and Thomas, G. (2004) *Mol. Cell. Biol.* **24,** 3112–3124
10. Shahbazian, D., Roux, P. P., Mieulet, V., Cohen, M. S., Raught, B., Taunton, J., Hershey, J. W., Blenis, J., Pende, M., and Sonenberg, N. (2006) *EMBO J.* **25,** 2781–2791
11. Aguilar, V., Alliouachene, S., Sotiropoulos, A., Sobering, A., Athea, Y., Djouadi, F., Miraux, S., Thiaudière, E., Foretz, M., Viollet, B., Diolez, P., Bastin, J., Benit, P., Rustin, P., Carling, D., Sandri, M., Ventura-Clapier, R., and Pende, M. (2007) *Cell Metab.* **5,** 476–487
12. Le Bacquer, O., Petroulakis, E., Paglialunga, S., Poulin, F., Richard, D., Cianflone, K., and Sonenberg, N. (2007) *J. Clin. Invest.* **117,** 387–396
13. Um, S. H., Frigerio, F., Watanabe, M., Picard, F., Joaquin, M., Sticker, M., Fumagalli, S., Allegrini, P. R., Kozma, S. C., Auwerx, J., and Thomas, G. (2004) *Nature* **431,** 200–205
14. Harada, H., Andersen, J. S., Mann, M., Terada, N., and Korsmeyer, S. J. (2001) *Proc. Natl. Acad. Sci. U.S.A.* **98,** 9666–9670
15. Janelidze, S., Hu, B. R., Siesjö, P., and Siesjö, B. K. (2001) *Neurobiol. Dis.* **8,** 147–154
16. Martín de la Vega, C., Burda, J., Nemethova, M., Quevedo, C., Alcázar, A., Martín, M. E., Danielisova, V., Fando, J. L., and Salinas, M. (2001) *Biochem. J.* **357,** 819–826
17. Mengesdorf, T., Proud, C. G., Mies, G., and Paschen, W. (2002) *Exp. Neurol.* **177,** 538–546
18. Jonassen, A. K., Mjøs, O. D., and Sack, M. N. (2004) *Biochem. Biophys. Res. Commun.* **315,** 160–165
19. Benavides, A., Pastor, D., Santos, P., Tranque, P., and Calvo, S. (2005) *Glia* **52,** 261–275
20. McCarthy, K. D., and de Vellis, J. (1980) *J. Cell Biol.* **85,** 890–902
21. Caso, J. R., Pradillo, J. M., Hurtado, O., Lorenzo, P., Moro, M. A., and Lizasoain, I. (2007) *Circulation* **115,** 1599–1608
22. Pérez-Asensio, F. J., Hurtado, O., Burguete, M. C., Moro, M. A., Salom, J. B., Lizasoain, I., Torregrosa, G., Leza, J. C., Alborch, E., Castillo, J., Knowles, R. G., and Lorenzo, P. (2005) *Neurobiol. Dis.* **18,** 375–384
23. Livak, K. J., and Schmittgen, T. D. (2001) *Methods* **25,** 402–408
24. Pérez-Ortiz, J. M., Tranque, P., Vaquero, C. F., Domingo, B., Molina, F., Calvo, S., Jordán, J., Cena, V., and Llopis, J. (2004) *J. Biol. Chem.* **279,** 8976–8985
25. Mieulet, V., Roceri, M., Espeillac, C., Sotiropoulos, A., Ohanna, M., Oorschot, V., Klumperman, J., Sandri, M., and Pende, M. (2007) *Am. J. Physiol. Cell Physiol.* **293,** C712–C722
26. Patel, S., Lochhead, P. A., Rena, G., Fumagalli, S., Pende, M., Kozma, S. C., Thomas, G., and Sutherland, C. (2002) *J. Biol. Chem.* **277,** 9889–9895
27. Alliouachene, S., Tuttle, R. L., Boumard, S., Lapointe, T., Berissi, S., Germain, S., Jaubert, F., Tosh, D., Birnbaum, M. J., and Pende, M. (2008) *J. Clin. Invest.* **118,** 3629–3638
28. Ohanna, M., Sobering, A. K., Lapointe, T., Lorenzo, L., Praud, C., Petroulakis, E., Sonenberg, N., Kelly, P. A., Sotiropoulos, A., and Pende, M. (2005) *Nat. Cell Biol.* **7,** 286–294
29. Pende, M. (2006) *Bull. Cancer* **93,** E39–E43
30. DeGracia, D. J. (2004) *J. Neurosci. Res.* **77,** 771–776
31. Jamison, J. T., Kayali, F., Rudolph, J., Marshall, M., Kimball, S. R., and DeGracia, D. J. (2008) *Neuroscience* **154,** 504–520
32. Althausen, S., Mengesdorf, T., Mies, G., Oláh, L., Nairn, A. C., Proud, C. G., and Paschen, W. (2001) *J. Neurochem.* **78,** 779–787
33. Pende, M., Kozma, S. C., Jaquet, M., Oorschot, V., Burcelin, R., Le Marchand-Brustel, Y., Klumperman, J., Thorens, B., and Thomas, G. (2000) *Nature* **408,** 994–997
34. Ruvinsky, I., and Meyuhas, O. (2006) *Trends Biochem. Sci.* **31,** 342–348
35. Chen, X. Q., Lau, L. T., Fung, Y. W., and Yu, A. C. (2005) *J. Neurosci. Res.* **79,** 798–808
36. Bambrick, L., Kristian, T., and Fiskum, G. (2004) *Neurochem. Res.* **29,** 601–608
37. Dugan, L. L., and Kim-Han, J. S. (2004) *J. Bioenerg. Biomembr.* **36,** 317–321
38. Volobouéva, L. A., Duan, M., Ouyang, Y., Emery, J. F., Stoy, C., and Giffard, R. G. (2008) *J. Cereb. Blood Flow Metab.* **28,** 1009–1016
39. Sulis, M. L., and Parsons, R. (2003) *Trends Cell Biol.* **13,** 478–483
40. Zhu, Y., Hoell, P., Ahlemeyer, B., Sure, U., Bertalanffy, H., and Krieglstein, J. (2007) *Neurochem. Int.* **50,** 507–516
41. Juhaszova, M., Zorov, D. B., Kim, S. H., Pepe, S., Fu, Q., Fishbein, K. W., Ziman, B. D., Wang, S., Ytrehus, K., Antos, C. L., Olson, E. N., and Sollott, S. J. (2004) *J. Clin. Invest.* **113,** 1535–1549
42. Desagher, S., Glowinski, J., and Premont, J. (1996) *J. Neurosci.* **16,** 2553–2562
43. Dringen, R., Gutterer, J. M., and Hirrlinger, J. (2000) *Eur. J. Biochem.* **267,** 4912–4916
44. Stolovich, M., Tang, H., Hornstein, E., Levy, G., Cohen, R., Bae, S. S., Birnbaum, M. J., and Meyuhas, O. (2002) *Mol. Cell. Biol.* **22,** 8101–8113
45. Shima, H., Pende, M., Chen, Y., Fumagalli, S., Thomas, G., and Kozma, S. C. (1998) *EMBO J.* **17,** 6649–6659
46. Richardson, C. J., Bröenstrup, M., Fingar, D. C., Jülich, K., Ballif, B. A., Gygi, S., and Blenis, J. (2004) *Curr. Biol.* **14,** 1540–1549
47. Pardo, O. E., Wellbrock, C., Khanzada, U. K., Aubert, M., Arozarena, I., Davidson, S., Bowen, F., Parker, P. J., Filonenko, V. V., Gout, I. T., Sebire, N., Marais, R., Downward, J., and Seckl, M. J. (2006) *EMBO J.* **25,** 3078–3088